MOLECULAR AND CELLULAR BIOLOGY, Sept. 2011, p. 3616–3629 Vol. 31, No. 17
0270-7306/11/$12.00 doi:10.1128/MCB.05164-11
Copyright © 2011, American Society for Microbiology. All Rights Reserved.

PERK Integrates Autophagy and Oxidative Stress Responses To Promote Survival during Extracellular Matrix Detachment▽

Alvaro Avivar-Valderas,[1] Eduardo Salas,[2] Ekaterina Bobrovnikova-Marjon,[3] J. Alan Diehl,[3] Chandandeep Nagi,[1] Jayanta Debnath,[2] and Julio A. Aguirre-Ghiso[1]*

Department of Medicine and Department of Otolaryngology, Tisch Cancer Institute, Black Family Stem Cell Institute, Mount Sinai School of Medicine, One Gustave L. Levy Place, New York, New York 10029[1]; University of California San Francisco, Department of Pathology, and Helen Diller Family Comprehensive Cancer Center, San Francisco, California 94143[2]; and Department of Cancer Biology and Abramson Cancer Research Institute, University of Pennsylvania School of Medicine, Philadelphia, Pennsylvania 19104[3]

Received 3 February 2011/Returned for modification 11 March 2011/Accepted 17 June 2011

Mammary epithelial cells (MECs) detached from the extracellular matrix (ECM) produce deleterious reactive oxygen species (ROS) and induce autophagy to survive. The coordination of such opposing responses likely dictates whether epithelial cells survive ECM detachment or undergo anoikis. Here, we demonstrate that the endoplasmic reticulum kinase PERK facilitates survival of ECM-detached cells by concomitantly promoting autophagy, ATP production, and an antioxidant response. Loss-of-function studies show that ECM detachment activates a canonical PERK-eukaryotic translation initiation factor 2α (eIF2α)-ATF4-CHOP pathway that coordinately induces the autophagy regulators ATG6 and ATG8, sustains ATP levels, and reduces ROS levels to delay anoikis. Inducible activation of an Fv2E-ΔNPERK chimera by persistent activation of autophagy and reduction of ROS results in lumen-filled mammary epithelial acini. Finally, luminal P-PERK and LC3 levels are reduced in PERK-deficient mammary glands, whereas they are increased in human breast ductal carcinoma *in situ* (DCIS) versus normal breast tissues. We propose that the normal proautophagic and antioxidant PERK functions may be hijacked to promote the survival of ECM-detached tumor cells in DCIS lesions.

The attachment of mammary epithelial cells (MECs) to the extracellular matrix (ECM) critically regulates survival, and upon ECM detachment they rapidly undergo cell death, commonly termed anoikis (11, 17). Studies of lumen formation in three-dimensional culture and of ductal elongation during mammary gland development both support a key role for anoikis in luminal clearance (10). Furthermore, anoikis resistance is proposed to promote filling of the normally hollow lumen in glandular epithelium, a hallmark of early breast cancers, such as ductal carcinomas *in situ* (DCIS) (11). Thus, there is significant interest in identifying the signals that induce anoikis resistance, as this may uncover new therapeutic targets that can be exploited to kill ECM-detached tumor cells.

Although the rapid activation of apoptotic pathways was originally proposed to drive anoikis, a growing body of evidence indicates that ECM-detached MECs simultaneously activate diverse cellular pathways that both positively and negatively impact anoikis (17). For example, recent work indicates that ECM-detached MECs show a rapid decrease in glucose intake, which correlates with a drop in ATP levels as well as the progressive accumulation of reactive oxygen species (ROS) (40). Thus, in order to survive the stresses of ECM detachment, epithelial cells must adapt to the concomitant reduction in energy levels and the progressive ROS-induced damage. Autophagy, a tightly regulated cellular self-digestion process, has emerged as one important adaptive mechanism that promotes cell survival during ECM detachment (16). Nonetheless, the pathways that allow detached cells to coordinate autophagy and oxidative stress relief, and thus promote the survival of ECM-detached cells, remain poorly understood.

Recently, we demonstrated that ECM-detached MECs robustly activate the endoplasmic reticulum (ER) kinase PERK (41). PERK is best studied during the accumulation of misfolded proteins in ER lumen (19), where its main function is to attenuate translation initiation by phosphorylating eIF2α at Ser51 (38). This in turn triggers a selective translation and transcription program that induces reversible growth arrest and allows cells to cope with ER stress, primarily by inducing an antioxidant response (8). Notably, PERK signaling has also been shown to induce autophagy as a survival pathway in response to several cellular insults, such as hypoxia, nutrient deprivation, or radiation (24, 33, 37, 39). Thus, a dual function is rendered by PERK, where transient growth arrest is coordinated with robust survival (2, 3, 14). This dual function is illustrated by pleiotropic roles of PERK during tumor progression. PERK can, via its growth-suppressive function, prevent or delay tumor formation (4, 41). However, when established tumors successfully bypass this growth restriction, cells take advantage of PERK activation to cope with ER stress and hypoxia present in the tumor mass (3). Accordingly, in ErbB2$^+$ mammary epithelium, the PERK antioxidant response favors tumor development (4).

Our recent work demonstrated that the activation of the

* Corresponding author. Mailing address: Department of Medicine and Department of Otolaryngology, Tisch Cancer Institute, Black Family Stem Cell Institute, Mount Sinai School of Medicine, One Gustave L. Levy Place, New York, NY 10029. Phone: (212) 241-9582. Fax: (212) 241-4096. E-mail: julio.aguirre-ghiso@mssm.edu.

▽ Published ahead of print on 27 June 2011.

canonical PERK-eukaryotic translation initiation factor 2α (eIF2α)-ATF4-CHOP pathway contributed to cell cycle withdrawal but did not promote anoikis (41). The aforementioned studies describing dual functions for PERK in growth arrest and cell survival motivated us to more closely dissect whether PERK mediated similar functions in ECM-detached cells. Here, we demonstrate that PERK activation in ECM-detached cells is responsible for coordinating both autophagy induction and oxidative stress relief, all of which are dependent on a canonical eIF2α-ATF4-CHOP pathway. In three-dimensional (3D) culture, the enforced activation of PERK results in the aberrant accumulation of cells that resist anoikis in the luminal space, indicating that this pathway must be turned off for proper luminal clearance. The tissue-specific deletion of PERK in the mouse mammary gland tissue results in reduced autophagy and increased apoptosis, whereas both PERK phosphorylation and autophagy are concomitantly increased in human DCIS. Based on these results, we propose that the proautophagic and antioxidant functions of PERK that operate during normal mammary acinus development are subverted in breast tumor cells for them to survive oxidative stress and resist anoikis.

MATERIALS AND METHODS

Cells lines and culture conditions. Low-passage MCF10A cells were cultured as described previously (12). For Fv2E-PERK stable cell lines, cells were treated with 100 pM AP20187 (AP) (added daily) or an equal volume of ethanol (vehicle) as a control. For anoikis assays, MCF10A cells were collected as described previously (41). After quantification, 4×10^5/ml of MCF10A cells were kept in ultra-low-attachment plates (Corning) with the appropriate growth medium at the indicated time and/or treated or transfected. Wild-type and PERK-knockout (KO) mouse embryo fibroblasts (MEFs) were kindly provided by David Ron (Cambridge University) and grown as described previously (19). For 3D cultures, cells were plated in commercially available growth factor-reduced Matrigel (Mgel) (BD Biosciences, San Diego, CA) and grown as described previously (12). For treatments and transfections during morphogenesis, 100 nM PERK or ATF4 small interfering RNA (siRNA) was supplemented every 24 h. To quantify cell viability, detached cells were washed with phosphate-buffered saline (PBS), disaggregated, and collected as a single-cell suspension using a cell-strained cap (BD Falcon) to be incubated in 1:2 trypan blue stain (BioWhittaker). Total and nonviable cells were manually determined using a counting chamber.

Reagents and plasmids. pBABEpuro-PERKΔC (lacking the PERK kinase domain) and pBABEpuro-Fv2E-PERK (where the modified FKBP [Fv] domain is fused to the PERK cytoplasmic kinase domain) were previously described (31). The pBABEpuro-β-galactosidase and -PERK-(K618A) constructs were described previously (41). The pCAG-EGFP-LC3 plasmid was a kind gift from Zhenyu Yue (Mount Sinai School of Medicine, New York, NY). AP20187 was from ARIAD Pharmaceuticals, Cambridge, MA, and salubrinal was from Calbiochem. When indicated, 10 nM bafilomycin A (BafA) (Sigma) was added to cells 1 h prior to lysis. Chloroquine (CQ) (Sigma) was used to block autophagosome maturation. Quantification of cellular ROS was performed using 2,7-dichlorofluorescein diacetate (DCF-DA) (Invitrogen). Ethidium bromide (EtBr) (Sigma) staining of 3D cultures was performed as described previously (12).

IB. MCF10A and MEFs were lysed, and protein was analyzed by immunoblotting (IB) as described previously (36). Membranes were blotted using antibodies against the following: P-PERK (Thr981), PERK, CHOP, and ATF4 (Santa Cruz Biotechnology); GAPDH (glyceraldehyde-3-phosphate dehydrogenase) and BimEL (Calbiochem); LC3 (Axxora, LLC) and BiP/Grp78 (BD Biosciences); cleaved caspase-3 (Asp175), eIF2α, P-eIF2α (Ser51), $p21^{Cip1}$, $p27^{KIP}$, P-GCN2 (Thr898), and GCN2 (Cell Signaling Technology); laminin 5 (Chemicon International); and p62 (Progen). Bound antibodies were detected with horseradish peroxidase (HRP)-conjugated secondary antibodies and chemiluminescence assays as described previously (41).

Real-time PCR primers. RNA was isolated from cells with TRIzol reagent following the manufacturer's instructions (Invitrogen). Reverse transcription was performed using Moloney murine leukemia virus (M-MuLV) reverse transcriptase (New England BioLabs). Real-time PCR was performed on a DNA Engine Opticon system using Power SYBR green PCR master mix. The human forward and reverse primer sequences used were as follows: ATG8, 5′-CATGAGCGAGTTGGTCAAGA-3′ and 5′-GGTTCACCAGCAGGAAGAAG-3′; ATG5, 5′-ATCCTGCAGAAGAAAATGGA-3′ and 5′-ACAGGACGAAACAGCTTCTG-3′; ATG6, 5′-GCGAGACACGTTTTTGTCTT-3′ and 5′-TGGGTTTTGATGGAATAGGA-3′; ATG7, 5′-GAACATGGTGCTGGTTTCCT-3′ and 5′-CATCCAGGGTACTGGGCTAA-3′; PERK, 5′-AGAAAAACTCCAGCCCAGTT-3′ and 5′-TCGTCCATTCATCCAGTCTT-3′; Glyt1, 5′-CAGCCCCAGCGAGGAGTACT-3′ and 5′-GAGACACCGAGGCAGCCAAG-3′; Slc3a2, 5′-ATTGGCCTGGATGCAGCTGC-3′ and 5′-ACAGCCCCTGGGATGTCAGG-3′; GAPDH, 5′-CCCCTGGCCAAGGTCATCCA-3′ and 5′-ACAGCCTTGGCAGCGCCAGT-3′; and ATF4 5′-CACTAGGTACCGCCAGAAGAAGA-3′ and 5′-AATCCGCCCTCTCTTTTAGAG-3′.

RNA interference (RNAi) and cDNA transfections. Cells were transiently transfected using Lipofectamine RNAiMax (Invitrogen) and FuGENE HD (Roche). DNA oligonucleotides encoding short hairpin RNA (shRNA) (the target sequence against ATG7 was CCC AGC TAT TGG AAC ACT GTA) were a kind gift from Jayanta Debnath (University of California, San Francisco). shRNA transfection was performed as described previously (16). Small interfering RNAs (siRNAs) were purchased from Ambion (CHOP, PERK, and silencer negative control), Dharmacon RNA Technologies (ATG7), or Invitrogen (ATF4). Transfections of plasmids and siRNA oligonucleotides were done using 3 μg DNA mixed with 6 μl of Fugene HD or 100 nM PERK, CHOP, or ATG7 siRNA oligonucleotides with 8 μl Lipofectamine RNAiMax and incubated for 24 and 48 h.

Fluorescence-activated cell sorting (FACS) analysis. For determination of percent apoptosis, 20,000 events were collected and the sub-G_0 fraction was measured using propidium iodide staining (BD Pharmingen). The sub-G_0 cell population was gated as the apoptotic fraction. Nonstained cells were used as negative control. For determination of percent ROS, cells were incubated in PBS containing 2 μM DCF-DA for 15 min, and then DCF-DA-positive cells were gated using nonstaining cells as a negative control.

Immunofluorescence and GFP-LC3 analysis and image acquisition. Alexa-Fluor- and rhodamine-conjugated secondary antibodies (Molecular Probes) were used for the 3D culture immunofluorescence assays. For detection of autophagosomes under adherent or suspension conditions, cells stably expressing green fluorescent protein (GFP)-LC3 MCF10A or transiently transfected cells were either grown on glass coverslips or collected by centrifugation for suspended cultures, allowed to attach on Poly-Prep slides (Sigma), and fixed with 3% paraformaldehyde following standard protocols (36). Images were captured using a Nikon Eclipse E600 microscope and an RT Slider SPOT digital camera (Diagnostic Instruments, Inc.). 3D-Matrigel MCF10A acinar structures were fixed at day 8, 10, 12, and 20 and processed for size measurement and immunofluorescence microscopy analysis as established previously (41). Confocal analyses were performed using a Leica SP5 multiphoton confocal microscope equipped with UV diode (405 nm), argon (458 nm, 476 nm, 488 nm, and 514 nm), HeNe (543 nm), and HeNe (633 nm) lasers. All images were taken using a magnification of ×63.

Animal tissues and immunohistochemistry. Mammary gland epithelium tissues were obtained from control $PERK^{loxP/loxP}$ and mammary gland-specific PERK knockout ($PERK^{\Delta/\Delta}$) mice generated as described previously (5). Immunohistochemistry on embedded paraffin sections was performed as described previously (41). The sections were processed using the VectaStain ABC Elite kit (Vector Laboratories, Burlingame, CA), and the signal was detected using the diaminobenzidine (DAB) substrate kit for peroxidase (Vector Laboratories, Burlingame, CA). P-PERK antibodies were from Santa Cruz, LC3 was from Axxora, and activated caspase-3 and P-GCN2 were from Cell Signaling.

Statistics. Statistical analysis was performed using GraphPad Prism 5.0 software (San Diego, CA), and *P* values were calculated using one-way analysis of variance (ANOVA) followed by the Bonferroni multiple-comparison posttest or the unpaired *t* test, with a *P* value of <0.05 considered statistically significant.

RESULTS

PERK activation in ECM-detached cells is linked to autophagy induction. We previously showed that PERK inhibits proliferation of ECM-bound MECs (41). However, we also discovered that PERK was strongly induced in suspended luminal cells (41), and this correlated with upregulation of CHOP. However, PERK inhibition via a PERKΔC mutant, while enhancing proliferation of ECM-attached MECs and

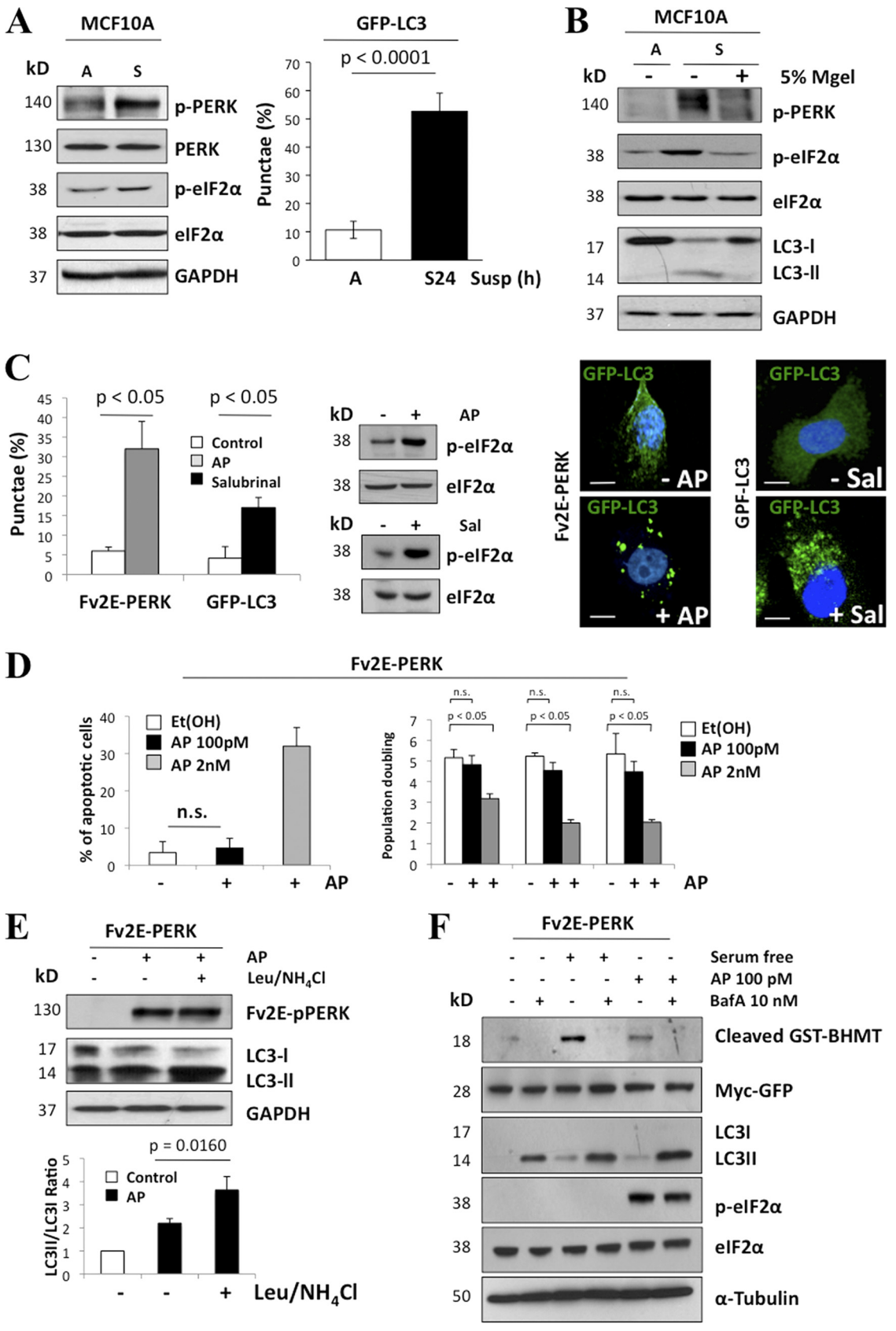
A
MCF10A
kD
A
S
140
p-PERK
130
PERK
38
p-eIF2α
38
eIF2α
37
GAPDH
GFP-LC3
p < 0.0001
Punctae (%)
A
S24
Susp (h)
B
MCF10A
A
S
kD
-
-
+
5% Mgel
140
p-PERK
38
p-eIF2α
38
eIF2α
17
LC3-I
14
LC3-II
37
GAPDH
C
p < 0.05
p < 0.05
Punctae (%)
Control
AP
Salubrinal
Fv2E-PERK
GFP-LC3
kD
AP
p-eIF2α
eIF2α
Sal
GFP-LC3
Fv2E-PERK
- AP
+ AP
GPF-LC3
- Sal
+ Sal
D
Fv2E-PERK
% of apoptotic cells
Et(OH)
AP 100pM
AP 2nM
n.s.
AP
Population doubling
n.s.
p < 0.05
E
Fv2E-PERK
AP
kD
Leu/NH4Cl
130
Fv2E-pPERK
17
14
LC3-I
LC3-II
37
GAPDH
p = 0.0160
LC3II/LC3I Ratio
Control
AP
Leu/NH4Cl
F
Fv2E-PERK
Serum free
AP 100 pM
kD
BafA 10 nM
18
Cleaved GST-BHMT
28
Myc-GFP
17
14
LC3I
LC3II
38
p-eIF2α
38
eIF2α
50
α-Tubulin

inhibiting CHOP induction in luminal cells, did not affect the rate of luminal cell apoptosis (41). We reasoned that PERK and CHOP might have a different function in the luminal compartment. Because ECM detachment can induce autophagy (16) and PERK can activate autophagy (24, 27, 34), we first tested whether PERK activation in suspension was responsible for autophagy induction. The substratum detachment of MCF10A cells enhanced both PERK and eIF2α phosphorylation (Fig. 1A), which correlated with autophagosome formation, as evidenced by increased numbers of cells exhibiting punctate GFP-LC3 (Fig. 1A, right panel) and increased phosphatidylethanolamine (PE) lipidation of endogenous LC3 (LC3-II) (Fig. 1B). Restoration of cell-ECM interactions due to the addition of laminin-rich reconstituted basement membrane (5% Matrigel) resulted in PERK and eIF2α deactivation and the inhibition of detachment-induced autophagy (Fig. 1B). In parallel, we tested whether PERK activation was sufficient to induce autophagy, using MCF10A cells engineered to express a construct in which the Fv2E dimerization domain is fused to the cytoplasmic kinase domain of PERK (Fv2E-PERK); this system allows for controlled PERK activation in the absence of fully activated ER stress via dimerization with the divalent small molecule AP20187 (AP) (31). Upon AP addition, PERK was robustly activated, resulting in increased autophagosome formation (Fig. 1C); remarkably, at the concentration of AP used (100 pM), we did not observe apoptosis or G_0-G_1 arrest (Fig. 1D). Furthermore, the induction of eIF2α phosphorylation with salubrinal, a small-molecule inhibitor of the GADD34-PP1c complex, also resulted in increased punctate GFP-LC3 (Fig. 1C) but had no significant effect on apoptosis (data not shown).

We next evaluated the lysosomal turnover of PE-lipidated LC3 (LC3-II) upon PERK activation to verify autophagic flux. Upon inhibition of lysosomal function, using either leupeptin plus ammonium chloride (Leu/NH_4Cl) or bafilomycin A (BafA), we observed enhanced LC3-II accumulation in AP-treated Fv2E-PERK MCF10A cells (Fig. 1D and E), thus corroborating that PERK activation promotes the lysosomal turnover of LC3-II. To further validate this result, we assessed the autophagy-dependent degradation of an exogenously provided cytoplasmic cargo protein (13). Fv2E-PERK cells were transfected with the macroautophagy reporter construct GST-BHMT (glutathione *S*-transferase fused to betaine homocysteine S methyltransferase 1) and treated with AP20187. Both serum withdrawal and AP-mediated activation of PERK promoted the lysosome-dependent cleavage of GST-BHMT (Fig. 1E). Chemical inhibition of autophagy with BafA, a vacuolar H^+-ATPase inhibitor, reverted GST-BHMT cleavage. Overall, these results demonstrate that PERK activation is sufficient to mediate both the formation and lysosomal turnover of autophagosomes as well as to drive autophagic proteolysis. Furthermore, in ECM-detached cells, PERK phosphorylation strongly correlates with autophagy induction and with the adhesive state of MCF10A cells.

PERK and eIF2α are required for detachment-induced autophagy. We subsequently assessed whether PERK activation is required for detachment-induced autophagy. As previously reported, the expression of a dominant-negative PERK mutant (PERKΔC, a kinase-dead C-terminal deletion mutant) (41) in MCF10A cells inhibited PERK autophosphorylation and eIF2α Ser51 phosphorylation during matrix detachment (Fig. 2A). Importantly, PERKΔC suspended cultures exhibited a 50% reduction in LC3-II compared to controls (β-galactosidase [β-Gal]). Thus, PERK kinase activity is required for LC3-I conversion to LC3-II (Fig. 2A). Accordingly, we also observed reduced LC3 lipidation in PERK-deficient mouse embryonic fibroblasts (Fig. 2B), suggesting that PERK regulation of autophagy is not limited to MCF10A cells. Moreover, siRNA-mediated depletion of PERK potently inhibited both eIF2α phosphorylation and detachment-induced autophagy in MCF10A cells; notably, the reduction in LC3-II was comparable to the inhibition of autophagy observed upon depletion of ATG7, a critical autophagy regulator (Fig. 2C). Thus, we conclude that both PERK kinase activity and the resultant eIF2α phosphorylation at Ser51 are at least partially responsible for detachment-induced autophagy.

PERK-dependent induction of ATG genes in suspension is mediated by ATF4 and CHOP. Phosphorylation of eIF2α, translation repression, and selective translation of the transcription factor (TF) ATF4 are central events in the unfolded-protein response (UPR) (20). ATF4 in turn induces the TF CHOP/GADD153 (1), a key mediator of the UPR. Notably,

FIG. 1. PERK activation in ECM-detached cells is associated with autophagy induction. (A) Whole-cell lysates from MCF10A cells adhered (A) or suspended for 24 h (S) and immunoblotted (IB) with indicated antibodies (Abs). The graph shows the percentage of autophagic (autophagosome puncta staining) MCF10A GFP-LC3 adhered or 24 h suspended cells. (B) Adhered (A) or suspended (S) MCF10A cells were treated or not treated with 5% Matrigel (MGel), and LC3 processing was detected by IB. (C) Adhered Fv2E-ΔNPERK MCF10A cell lines were transfected with GFP-LC3 plasmid and treated or not treated (control) with 100 pM AP10287 (AP) (dimerizing molecule) for 24 h, or adhered GFP-CL3 MCF10A cells were treated or not treated (control) with 100 nM salubrinal; cells were fixed and the percentage of autophagic cells was scored and quantified using fluorescence microscopy. The right panels show representative images of autophagic Fv2E-ΔNPERK (+AP) and GFP-LC3 (+Sal) MCF10A cells. Blue, 4′,6′-diamidino-2-phenylindole (DAPI); green, GFP-LC3. Scale bars are 5 μm. (D) Adhered Fv2E-ΔNPERK MCF10A cell line transfected with GFP-LC3 plasmid and treated with 100 pM or 2 nM AP or with vehicle [Et(Oh)] for 24 h were stained with EtBr, and the percentage of apoptotic cells was further measured by FACS. Right graph, population doubling during exponential growth (from day 2 to 8) of Fv2E-ΔNPERK MCF10A cells treated with vehicle (ethanol) or 100 pM or 2 nM AP. Cells were collected, and viability was determined using trypan blue exclusion. n.s., not significant. (E) Whole-cell lysates from Fv2E-ΔNPERK MCF10A cells treated or not treated with 100 pM AP and in combination with 0.1 mM leupeptin and 20 mM NH_4Cl as indicated were analyzed by IB for the indicated antigens. Leupeptin- and NH_4Cl-mediated inhibition of lysosomal degradation resulted in LC3-II accumulation (lane 3). Densitometric analysis (bottom panel) for LC3 flux was determined using Image J software ($n = 3$). (F) MCF10A cells were transfected with 5 μg cDNA encoding GST-BHMT (glutathione *S*-transferase fused to betaine homocysteine S methyltransferase 1). After 24 h, the cells were cultured in full growth medium, serum-free medium (6 h), or medium with AP20185 (100 pM) in the presence or absence of 10 nM bafilomycin A1 (BafA). Whole-cell lysates were immunoblotted for the indicated antigens. Myc Ab was used to detect GFP-myc (expressed from an internal ribosome entry site [IRES] sequence) as a control for transfection efficiency.

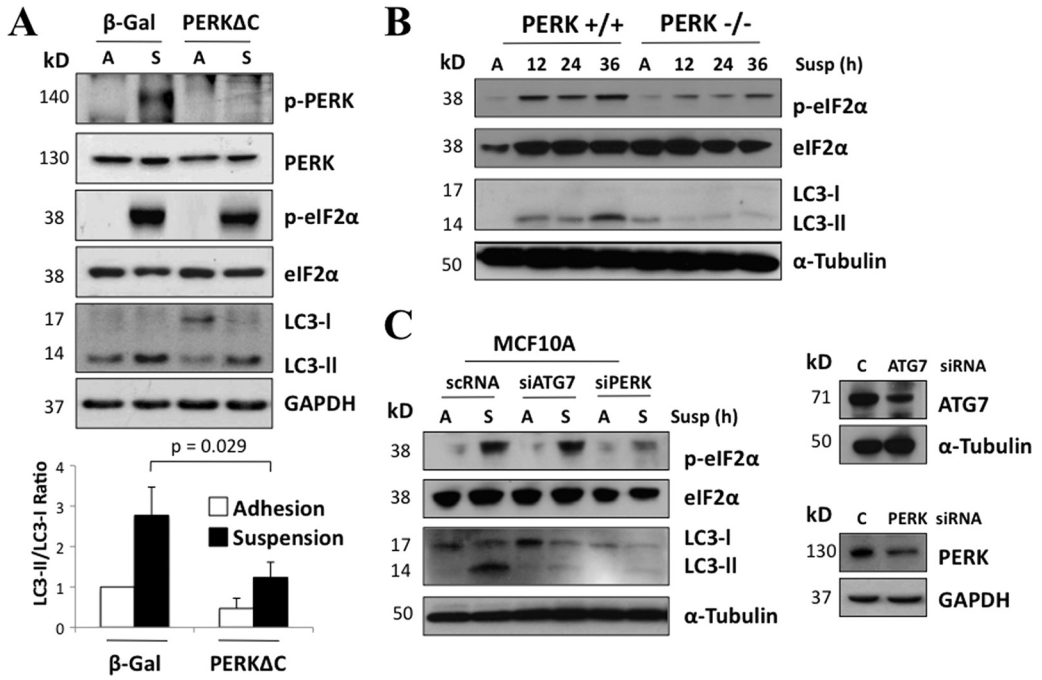

FIG. 2. PERK inhibition partially reverts suspension-induced autophagy. (A) Lysates from adhered (A) or 6 h suspended (S) β-Gal and PERKΔC MCF10A cells were analyzed by IB for the indicated antigens. Densitometric analysis for LC3 flux was done using Image J software (n = 3). (B) Lysates of *PERK*$^{+/+}$ and *PERK*$^{-/-}$ mouse embryonic fibroblasts (MEFs) were collected at the indicated time points, and the indicated antigens were detected by IB. (C) MCF-10A lysates from attached (A) and suspended (S) cells that were transfected with ATG7, PERK, or control (C) siRNA were used for IB against the indicated antigens. Results for the ATG7 and PERK knockdown controls are shown in the right panel.

both ATF4 and CHOP were implicated as potential transcriptional mediators in autophagy (32, 37). Thus, we hypothesized that these PERK/eIF2α-dependent transcriptional pathways may contribute to autophagy. In support of this, RNAi-mediated depletion of PERK, ATF4, and CHOP prevented suspension-induced LC3-II formation (Fig. 3A). Furthermore, expression of the PERKΔC mutant strongly reduced the mRNA levels of ATG8/LC3 and ATG5 under attached conditions (Fig. 3B). In addition, upon 6 h of detachment, MCF10A cells expressing the PERKΔC mutant or a kinase-dead K618A-PERK mutant showed an impaired ability to induce ATG6/Beclin-1 mRNA compared to controls (Fig. 3C). A similar inhibition of ATG6/Beclin-1 mRNA induction was observed in MCF10A cells expressing an eIF2α S51A mutant (Fig. 3C), as well as during ATF4 and PERK knockdown (Fig. 3D). Notably, Fv2E-ΔNPERK activation with AP was also able to drive transcriptional upregulation of ATF4, CHOP, and ATG6/Beclin1 under adhered conditions (Fig. 3E). These data suggest that in addition to ATG8/LC3 processing, PERK and eIF2α phosphorylation result in upregulation of ATF4 and CHOP (41), which contributes to the transcription of ATG6 mRNA as well as LC3 processing in suspended cells, respectively.

Enforced activation of PERK induces luminal space filling. To gain greater insight into PERK control of autophagy, we monitored the kinetics of PERK activation during MCF10A acinus morphogenesis. Both the total protein levels and phosphorylation of PERK became detectable at day 4 of 3D culture, peaked at day 6, and then significantly diminished at day 8 and thereafter; importantly, these changes were associated with increased phosphorylation of eIF2α at Ser51 (Fig. 4A). Furthermore, at these time points, we did not detect any changes in the PERK mRNA levels (Fig. 4A) or observe any changes in other ER-resident protein such as Bip/Grp78 (data not shown). We did observe a slight decrease in GCN2 and calnexin protein levels at later time points of acinus morphogenesis (Fig. 4A, right panel). The timing of PERK activation and upregulation coincided with luminal clearance and with Beclin1/ATG6 induction, which was strongly induced at day 4 of morphogenesis (Fig. 4A, upper right panel). ECM-detached luminal cells (arrow) strongly induced autophagy as measured by LC3-GFP imaging in 3D cultures (Fig. 4A, lower right panel). We also found that ECM-bound acinar basal cells (arrowheads) also had basal autophagy (Fig. 4A, lower right panel). It is possible that this is basal autophagy or that those cells are in the process of detachment. Next, we tested the consequence of enforced PERK activation during acinus morphogenesis using the Fv2E-ΔNPERK MCF10A system to sustain PERK activation beyond day 8. Fv2E-ΔNPERK activation with 100 pM AP resulted in a significant increase in overall acinus cell numbers and filling of the luminal space (Fig. 4B). However, this did not significantly enhance acinus size (Fig. 4B, upper right panel) or profoundly disrupt the spherical architecture of individual acini (data not shown).

Next, we tested whether PERK-induced luminal occupancy correlated with decreased apoptosis in luminal cells. Fv2E-ΔNPERK-mediated activation of PERK correlated with a consistent reduction of ethidium bromide (EtBr)-, cleaved-caspase-3- and BimEL-positive acinar luminal cells (Fig. 4C and D). PERK-induced survival was dependent on ATF4, be-

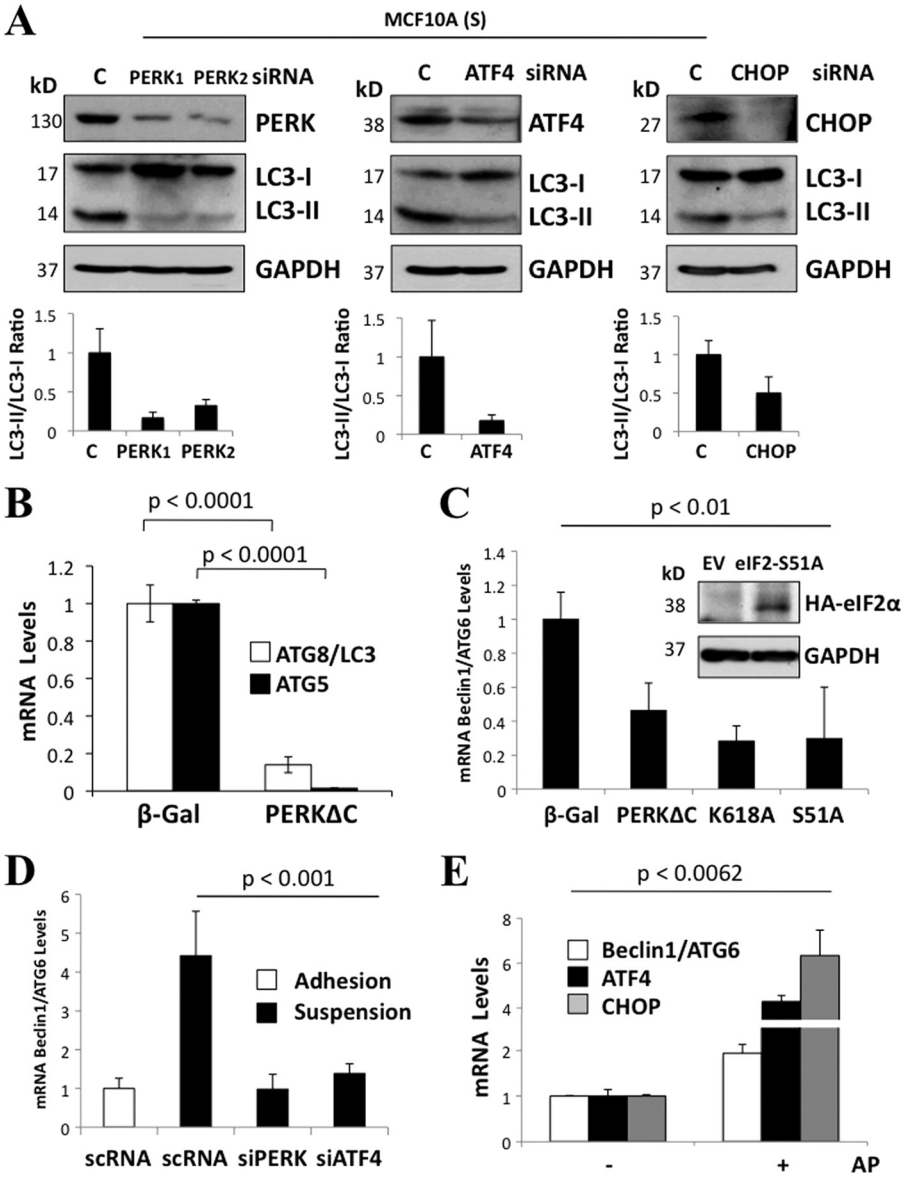

FIG. 3. Phosphorylation of PERK and eIF2α at Ser51 is required for efficient induction of ATG genes during suspension. (A) Lysates from MCF10A cells were suspended for 6 h (S) and transfected with PERK 1, PERK 2, ATF4, CHOP, and scRNA (C) siRNAs and immunoblotted for the indicated antigens. The graphs below the blots show densitometric analysis for LC3-II/LC3-I ratios as quantified using Image J software ($n = 3$). (B to E) Graphs showing quantitative PCR (qPCR) analysis of ATG8/LC3 and ATG5 mRNA transcript levels from β-Gal and PERKΔC MCF10A cells (B), Beclin1/ATG6 mRNA transcript levels from β-Gal, PERKΔC, PERK kinase-dead mutant K618A (K618A), and S51A-eIF2α mutant (S51A) suspended MCF10A cultures. (C) The inset shows a control IB of MCF10A cells stably expressing pBabepuro-HA-eIF2αS51A mutant or the empty vector (EV), which were immunoblotted with hemagglutinin (HA) and GAPDH (glyceraldehyde-3-phosphate dehydrogenase) Abs. (D and E) Beclin1/ATG6 mRNA transcript levels in adhered and suspended cultures transfected with PERK, ATF4, and control (C) siRNAs (D) and CHOP, ATF4, and Beclin1/ATG6 mRNA transcripts levels of Fv2E-PERK with (+) or without (−) 100 pM AP for 24 h (E). GAPDH mRNA was used for normalization.

cause RNAi-mediated reduction of this TF restored the formation of hollow acini in the setting of AP-mediated PERK activation (Fig. 4E). This suggests that PERK-ATF4 signaling transiently inhibits anoikis, allowing for transient survival of luminal cells devoid of ECM attachment.

Following lumen formation, excess cells are produced due to low-level proliferation within acini that continue to be cleared via luminal apoptosis (11). To test whether PERK activation enhanced the survival of ECM-detached cells during these late stages of morphogenesis, we treated Fv2E-ΔNPERK MCF10A acini with AP after day 12, a time point when luminal clearance is complete (21). Following 8 days of AP treatment, these structures displayed high numbers of intraluminal cells compared to nontreated controls (Fig. 4F). Remarkably, we also observed a significant increase in the number of basal-layer cells (Fig. 4F, right panels). This was not due to increased luminal cell proliferation or general proliferation, because in 2D cultures 100 pM AP had no significant effect on cell pro-

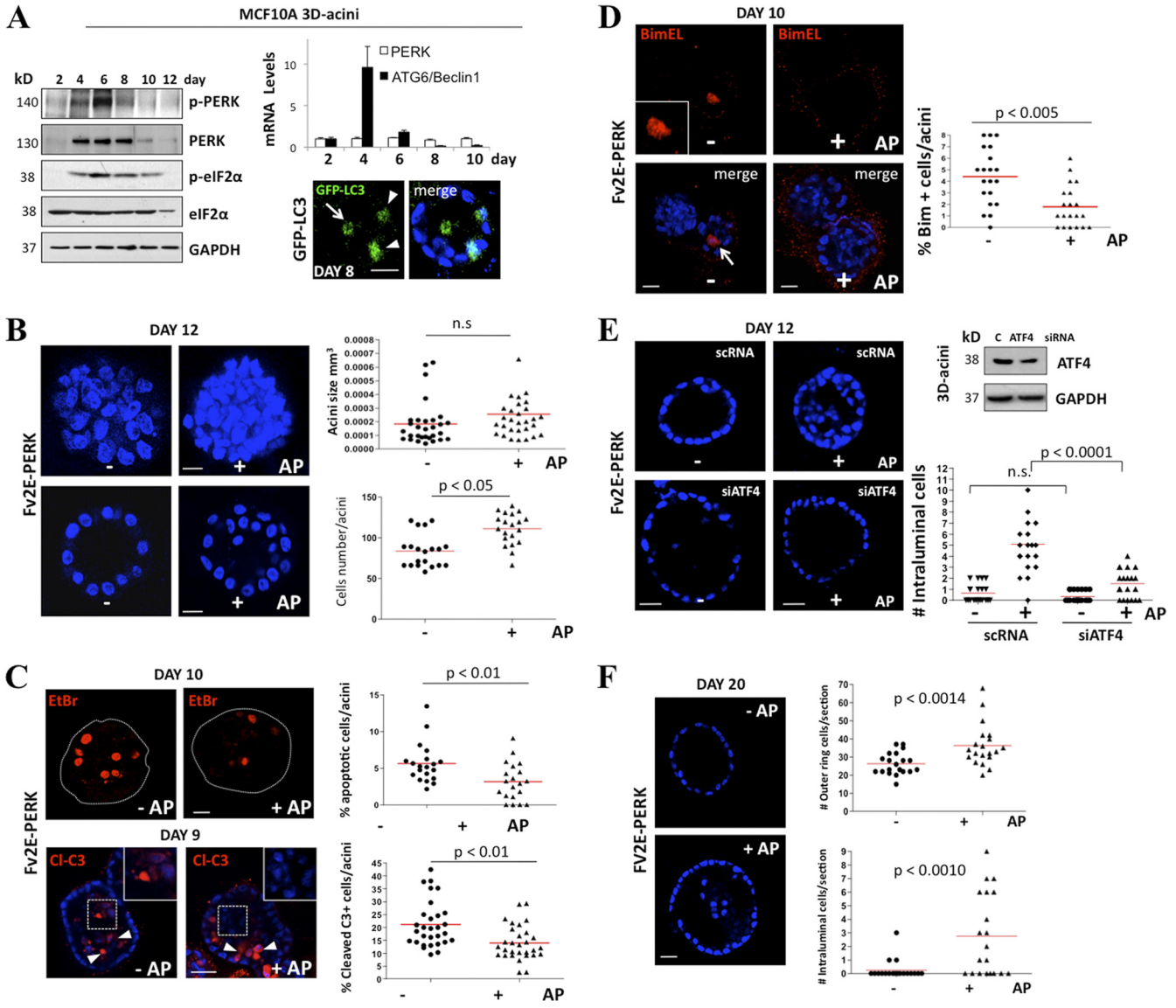

FIG. 4. Unscheduled activation of PERK induces luminal space filling. (A) Whole-cell lysates from 2- to 12-day-old MCF10A acini were immunoblotted with the indicated Abs. The upper right panel shows PERK and Beclin1/ATG6 mRNA transcript levels normalized to GAPDH mRNA from 3D Matrigel acini collected at the indicated time points. Confocal equatorial images from GFP-LC3 (the distribution of LC3-positive events is quantified in Fig. 5A) MCF10A acini fixed at day 8 show punctate basal (arrowheads) and luminal (arrow) LC3 staining (green). Blue, DAPI. Scale bars are 25 μm. (B) Confocal images of day 12 MCF10A Fv2E-ΔNPERK acini treated from day 6 to day 12 (+) or not treated (−) with 100 pM AP, showing stacked sections to reveal increased cellularity and compaction (upper panels) or equatorial confocal sections of acini (lower panels). The graph (upper right panel) shows the distribution and mean size of day 12 MCF10A Fv2E-ΔNPERK acini treated from day 6 (+) or not treated (−) with 100 pM AP. Size was calculated using SPOT software following the equation [(length × width^2)/2 = acinus volume (mm^3)] (n = 50). The total number of cells per acinus (lower right panel) was also calculated (n = 50). (C) Fv2E-ΔNPERK acini treated from day 6 to days 9 and 10 (+) or not treated (−) with 100 pM AP were stained with 1 μg/ml EtBr (day 10) or cleaved caspase-3 (Cl-c3) at day 9. Magnifications show intraluminal Cl-c3 staining in nontreated acini versus negative Cl-c3 staining in AP-treated acini. The percentage of apoptotic cells was scored (right graphs) (n = 40). (D) Confocal equatorial images from Fv2E-ΔNPERK MCF10A acini treated from day 6 to day 12 (+) or not treated (−) with 100 pM AP, showing intraluminal BimEL staining (red). The graph shows the distribution and mean number of intraluminal BimEL-positive cells per acinus. (E) Confocal equatorial images from Fv2E-ΔNPERK acini treated from day 6 to day 12 (+) or not treated (−) with 100 pM AP and transfected with ATF4 or control (scRNA) siRNA. The right graph show the distribution and mean number of intraluminal cells for each equatorial section of a single acinus (n = 20). Scale bar = 10 μm. The right blot shows controls for ATF4 knockdown in the 3D cultures. (F) Equatorial confocal section images of day 20 MCF10A Fv2E-ΔNPERK acini treated from day 6 to day 20 (+) or not treated (−) with 100 pM AP, showing intraluminal filling (left panels). Graphs (right panels) show the mean number and distribution of cells in the outer ring per section (upper panel) and the total number of intraluminal cells per section (lower panel) (n = 50). In all of the images blue shows DAPI staining of nuclear DNA, and unless otherwise indicated, scale bars indicate 25 μm. P values were determined by the t test.

liferation (Fig. 1D). Furthermore, at day 20, when acini normally exhibit proliferation arrest, no phospho-RB-positive cells were detected in either control or AP-treated Fv2E-ΔNPERK MCF10A acini (data not shown), thus supporting the idea that enhanced proliferation does not contribute to increased acinus size (Fig. 4F). Importantly, recent work demonstrates that MECs in the basal compartment are motile; they can detach into the luminal space and subsequently reattach to the ECM (35). Based on our results, we speculate that MECs that survive and persist in the luminal space due to PERK activation may be repositioned to the basal layer. Overall, the persistent unscheduled activation of PERK promotes lumen occupancy and increased numbers of cells in the basal ECM-attached layer.

Autophagy contributes to luminal filling mediated by PERK activation. Autophagy is a prosurvival mechanism that can transiently protect cells from ECM detachment, provided that they reattach in a timely manner (30). Thus, we tested whether PERK-induced autophagy contributes to its ability to promote the luminal cell survival mechanism during acinus morphogenesis. Using Fv2E-ΔNPERK MCF10A cells stably expressing GFP-LC3, we found that AP-mediated activation of Fv2E-ΔNPERK significantly enhanced punctate GFP-LC3 within cells (Fig. 5A). Notably, PERK-stimulated LC3 processing was confined to cells occupying the luminal space (Fig. 5A, middle panel). In addition to LC3 processing, Fv2E-ΔNPERK activation in the acini increased the mRNA expression of several ATG genes, such as ATG7/8 and ATG6/Beclin1 (Fig. 5A, right panel). Importantly, treatment with the autophagy inhibitor chloroquine (CQ), which prevents the fusion of autophagosomes and lysosomes (25), completely reversed PERK-mediated accumulation of luminal cells and filling of this compartment in the AP-treated acini (Fig. 5B). Furthermore, shRNA-mediated downregulation of ATG7, which was previously shown to mediate luminal cell survival (16) and is induced by PERK (Fig. 5A), also resulted also in the reversion of luminal cell accumulation mediated by PERK (Fig. 5C). These results support the idea that autophagy contributes to the accumulation of luminal cells observed upon PERK activation.

Luminal cell autophagy and survival induced by PERK is accompanied by oxidative stress relief. Both suspension-induced phosphorylation of PERK and autophagosome formation were abrogated by treatment with the reducing agent *N*-acetyl-L-cysteine (NAC) (Fig. 6A and B), suggesting that ROS production was a trigger for PERK activation as well as autophagy. Recent publications indicate that competing ROS-induced-death-promoting (40) and autophagy-dependent survival (16) signals are simultaneously activated in luminal ECM-detached cells. Thus, we hypothesized that PERK activation in response to increased ROS may simultaneously coordinate autophagy induction and ROS detoxification in ECM-detached cells. ROS production upon ECM-detachment was reversed by adding 5% Matrigel (Mgel) to suspension cultures (Fig. 6C, left panel). Thus, the disruption of adhesion signaling is responsible for both ROS production and PERK activation. Accordingly, inhibition of the canonical PERK/eIF2α signaling pathway via expression of the PERKΔC or S51D-eIF2α mutant strongly increased ROS levels as measured by DCF-DA fluorescence in suspended MCF10A cells (Fig. 6C, right panel). Because ROS accumulation in ECM-detached MECs is associated with reduced ATP levels, we assessed whether PERK activity modulated ATP levels in suspended MECs (40). Upon siRNA-mediated knockdown of PERK, we uncovered a more precipitous drop in ATP levels than in control suspension cultures (Fig. 6D, left panel). In contrast, AP-mediated activation of PERK was able to partially maintain ATP levels in ECM-detached cells (Fig. 6D, right panel). Importantly, we found that ROS were detectable in both basal and centrally localized cells of control Fv2E-ΔNPERK 3D acinar structures (Fig. 6E). However, AP-mediated activation of PERK drastically reduced ROS production in both compartments (Fig. 6E). Overall, these results indicated that PERK/eIF2α signaling is important to reduce oxidative stress due to the loss of adhesion. In further support of this, two ATF4 target genes specifically implicated in ROS detoxification, Glyt1 and Slc3a2, were induced in AP Fv2E-PERK-treated acini (Fig. 6E, lower right panel). Expression of the mRNA of Slc3a2 peaked at day 6 of morphogenesis, when PERK activity peaks (Fig. 4A and 6F), and remained high until day 12. Overall, these data support an antioxidant role for PERK during morphogenesis and strongly suggest that the ROS-detoxifying function of PERK→ATF4 signaling is induced concomitantly with autophagy in mammary acini.

Next, we investigated the effects of PERK on cell survival during ECM detachment. PERK inhibition using the PERKΔC mutant significantly reduced viability after 6 h in suspension (Fig. 6G), and this correlated with induction of BimEL and increased caspase-3 processing (data not shown). PERK-mediated regulation of BimEL was not associated with changes in ERK1/2 activation (data not shown). ATF4 RNAi also induced BimEL expression and caspase-3 activation in suspension, while Fv2E-PERK activation attenuated these effects (data not shown). Similarly, PERK inhibition using the ΔC and K618A mutants also resulted in reduced clonogenic plating efficiency of cells after 6 h in suspension (Fig. 6H). In contrast, Fv2E-ΔNPERK activation enhanced the plating efficiency of cells following detachment (Fig. 6H, right panel). Notably, these prosurvival functions of PERK during ECM detachment were temporally limited; beyond 8 h in suspension, both PERKΔC mutant and Fv2E-ΔNPERK activation showed no significant differences in BimEL levels and in plating efficiency versus β-Gal or inactive Fv2E-ΔNPERK controls (data not shown). We conclude that in ECM-detached MECs, the canonical PERK/eIF2α/ATF4 pathway promotes autophagy and ROS reduction, which transiently protects MECs lacking cell-ECM contact, provided that they reattach in a timely manner.

PERK promotes autophagy and survival in lactating mammary glands. Collectively, our data suggest that PERK-induced autophagy, ROS detoxification, and survival of luminal MECs may be important during mammary morphogenesis. To test this possibility, we examined the expression levels of LC3 and BimEL using immunohistochemistry in mammary gland sections from lactating female mice (L12) that carried wild-type (wt) *PERK* (*PERK*$^{loxP/loxP}$) or in which PERK was conditionally deleted (*PERK*$^{\Delta/\Delta}$) in the mammary tissue. We focused our studies on this developmental stage because the expanded ducts of lactating mammary glands facilitate the detection of luminal cells undergoing anoikis, which would be difficult to detect in virgin tissues or masked by the massive wave apoptosis observed during involution. As expected, a strong P-PERK signal in wt *PERK* tissues was lost in *PERK*$^{\Delta/\Delta}$ mam-

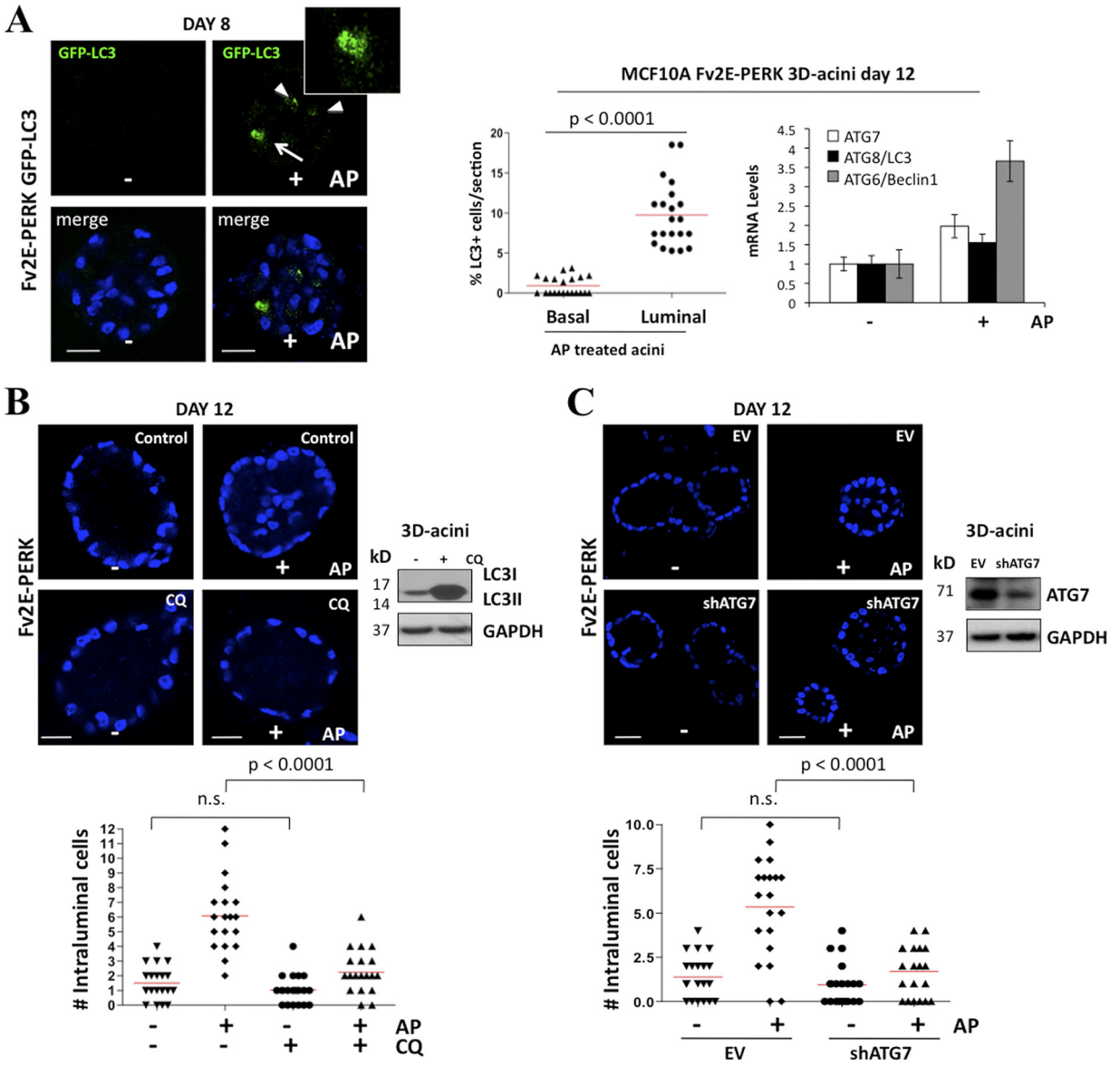

FIG. 5. PERK promotes survival in the luminal compartment via autophagy. (A) Representative confocal images of day 8 Fv2E-ΔNPERK and GFP-LC3 MCF10A acini treated from day 6 to 8 (+) or or not treated (−) with 100 pM AP, showing intraluminal LC3-puncta staining within cells (green). Middle panel, percentage of intraluminal LC3-puncta staining cells ($n = 50$); right panel, graph showing ATG gene mRNA transcript levels (middle panel) normalized to GAPDH. (B and C) Confocal equatorial images from Fv2E-ΔNPERK acini treated from day 6 to day 12 (+) or or not treated (−) with 100 pM AP and/or 20 μM chloroquine (CQ) (B) or shRNA ATG7 or control empty vector (EV) (C). The lower graphs show the distribution and mean number of intraluminal cells for each equatorial section of a single acinus ($n = 20$). Scale bar = 10 μm. Right blots show controls for CQ inhibition of autophagy (B) and ATG7 knockdown (C) in the 3D cultures. In all of the images, blue indicates DAPI staining of nuclear DNA, and unless otherwise indicated, scale bars indicate 25 μm. *P* values were determined by the *t* test.

mary glands (Fig. 7A). Strikingly, we found that P-PERK levels were higher in both detached (Fig. 7A, middle row) and luminal (Fig. 7A, lower row) $PERK^{loxP/loxP}$ cells. Isotype controls demonstrated no noticeable immunohistochemical signal, supporting that the staining observed in Fig. 7 is specific (data available upon request). Phospho-GCN2 staining showed no difference between wt *PERK* and $PERK^{\Delta/\Delta}$ tissues, suggesting that there is no compensatory increase in GCN2 activation in response to PERK KO (data available upon request).

Importantly, the levels of LC3 were dramatically reduced in $PERK^{\Delta/\Delta}$ in comparison to $PERK^{loxP/loxP}$ tissues (Fig. 7B), suggesting that PERK deletion reduces the activation of autophagy in the mammary tissue. Paralleling P-PERK activation, LC3 levels were significantly enhanced in luminal $PERK^{loxP/loxP}$ cells (Fig. 7B, lower row); isotype-matched IgG controls showed no staining (data available upon request). In agreement with an impaired autophagic flux in $PERK^{\Delta/\Delta}$ mammary epithelium, we detected the strong punctate accumulation of p62/SQSTM1 (Fig. 7C), an established autophagy cargo receptor that accumulates as cytoplasmic bodies when autophagy is inhibited (26). In addition, we observed increased BimEL staining throughout the mammary epithelium in $PERK^{\Delta/\Delta}$ compared to

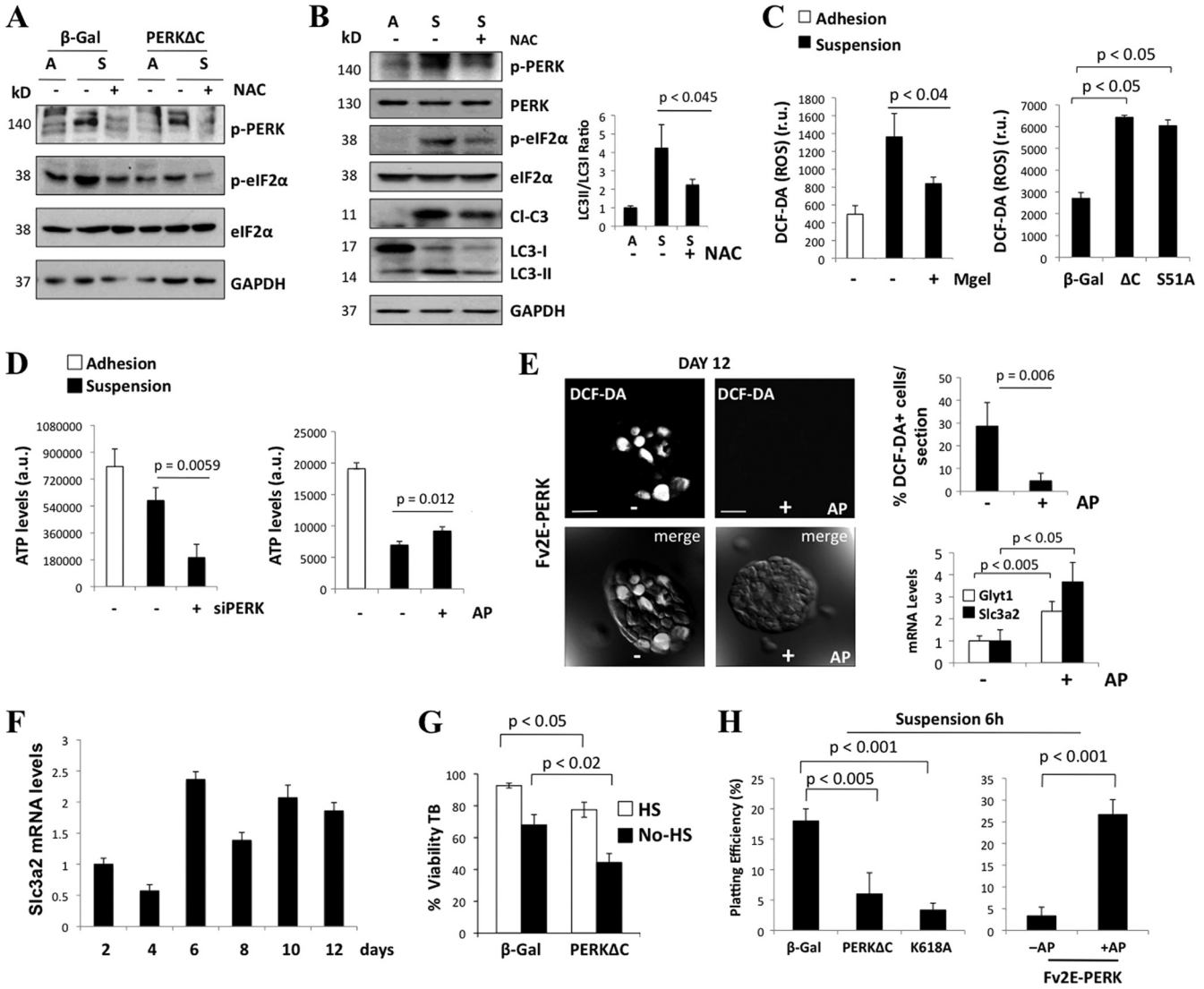

FIG. 6. PERK-eIF2α protects luminal cells from anoikis in part by relieving oxidative stress. (A) Whole-cell lysates from adhered (A) and 24-h-suspended (S) β-Gal and PERKΔC MCF10A cells were treated (+) or not treated (−) with 5 mM NAC and immunoblotted with the indicated Abs. GAPDH was used as a loading control. (B) Cell lysates from adhered (A) and 6-h-suspended (S) MCF10A cells were treated (+) or not treated (−) with 5 mM NAC and immunoblotted with the indicated Abs. Note that LC3 processing in suspension is inhibited by NAC treatment. Densitometric analysis (right panel) for LC3 flux was determined using Image J software ($n = 3$). (C) ROS levels of 6-h-suspended MCF10A cells cultured with (+) or without (−) 5% Matrigel and β-Gal. Levels for PERKΔC (ΔC) or eIF2α Ser51A (S/A) MCF10A cells were measured with DCF-DA and FACS. (D) ATP levels in adhered and 6-h-suspended MCF10A cells transfected with a PERK siRNA (+) or scrambled siRNA control (−) and in Fv2E-PERK MCF10A cells treated (+) or not treated (−) with 100 pM AP. (E) Confocal images from Fv2E-ΔNPERK MCF10A acini treated from day 6 to day 12 (+) or not treated (−) with 100 pM AP. At 15 min before confocal analysis, cells were treated with 2 μM DCF-DA. The lower panels show differential interference contrast (DIC) microscopy plus DCF-DA fluorescence. Upper right graph, quantification of DCF-DA-positive cells per equatorial section ($n = 7$). Lower right graph, qPCR analysis of Glyt1 and Slc3a2 mRNA transcript levels from Fv2E-ΔNPERK MCF10A acini treated from day 6 to day 12 (+) or not treated (−) with 100 pM AP and normalized to GAPDH mRNA. (F) qPCR analysis of Slc3a2 mRNA transcript levels from Fv2E-ΔNPERK MCF10A acini treated from day 6 to day 12 (+) or not treated (−) with 100 pM AP at the indicated time points. (G) β-Gal- and PERKΔC-MCF10A 6-h-suspended cultures grown in full or serum (HS)-free medium were analyzed for viability using the trypan blue (TB) exclusion test. (H) β-Gal, PERKΔC (ΔC), or K618A PERK MCF10A 6-h-suspended cultures were collected and assayed for plating efficiency. PERKΔC or K618A PERK mutants inhibited plating efficiency (left panel). Fv2E-ΔNPERK MCF10A 6-h-suspended cultures (right panel) treated with 100 pM AP (+) exhibited a higher plating efficiency than nontreated cultures (−). *P* values were determined by the *t* test.

$PERK^{loxP/loxP}$ tissues, which was most evident in luminal cells within $PERK^{\Delta/\Delta}$ ducts that were strongly stained for BimEL (Fig. 7D, upper and middle rows). This pattern suggested that PERK deletion is accompanied by increased cell death due to BimEL induction. Accordingly, $PERK^{\Delta/\Delta}$ tissues displayed significantly increased numbers of cleaved-caspase-3-positive luminal cells (Fig. 7D, lower rows). Collectively, these results support that PERK activation promotes autophagy as well as inhibits the induction of BimEL, which together promote the survival of MECs.

Enhanced PERK phosphorylation and LC3 expression in DCIS. The PERK antioxidant response and autophagy were

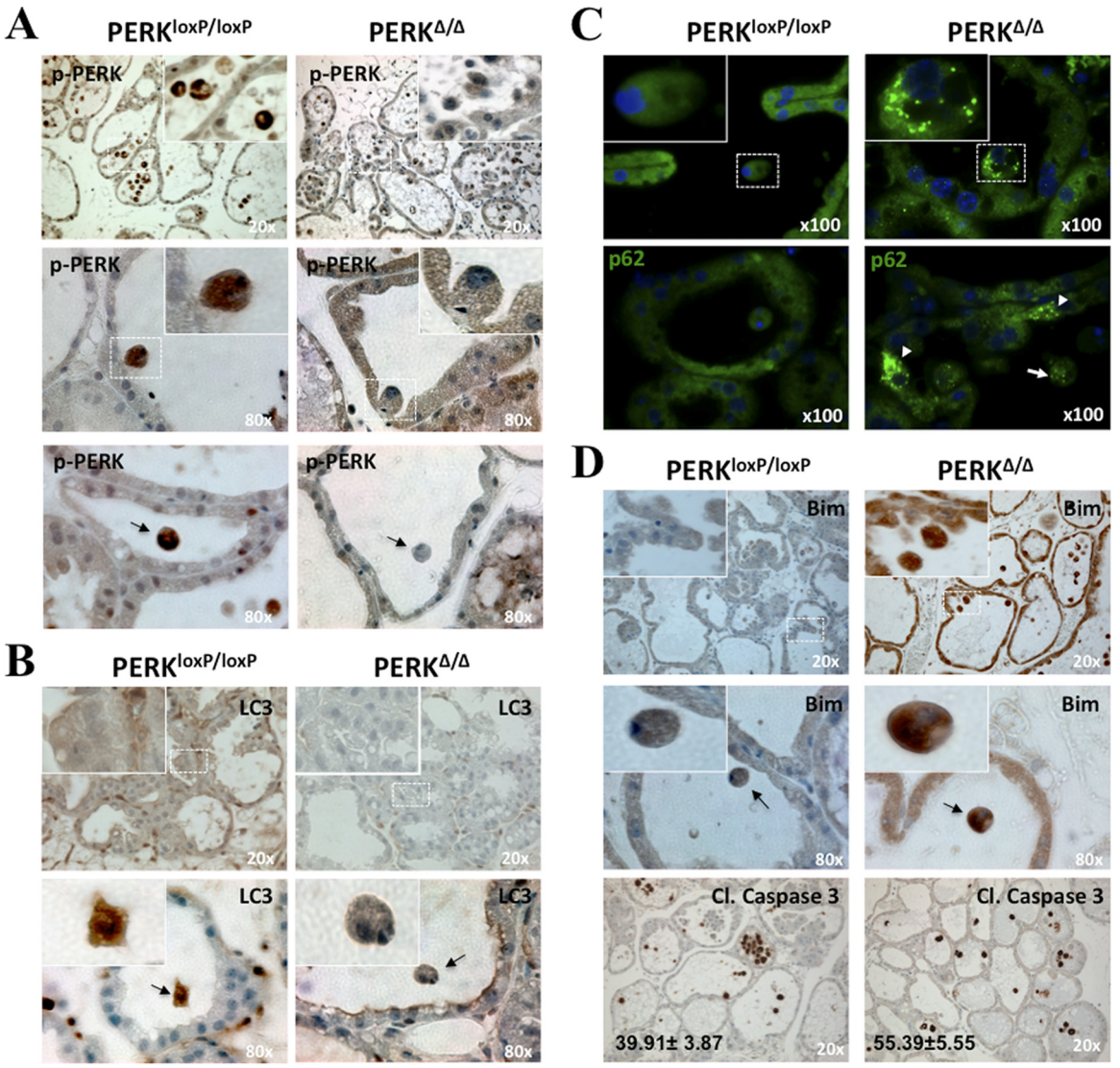

FIG. 7. PERK promotes autophagy and survival in lactating mammary glands. Detection of P-PERK (A), LC3 (B), p62 (C), and BimEL and cleaved caspase-3 (D) in day 12 lactating mammary glands sections from control $PERK^{loxP/loxP}$ and mammary gland-specific PERK knockout ($PERK^{\Delta/\Delta}$) mice was done by immunohistochemistry (A, B, and D) and immunofluorescence (C). (A) Images showing enhanced P-PERK staining in the control tissues along with strong staining in detaching (middle panels and insets) and luminal cells (arrow, lower panels), which is lost in $PERK^{\Delta/\Delta}$ tissues. (B) Images showing enhanced LC3 staining (upper panels and insets) and detachment-induced LC3 expression (lower panels) in $PERK^{loxP/loxP}$ control tissues, which is lost in $PERK^{\Delta/\Delta}$ tissues. (C) Images showing enhanced p62 punctate staining in $PERK^{\Delta/\Delta}$ versus control tissues. Insets show magnification to illustrate the accumulation of p62 in autophagosomes. Arrows show p62 punctate staining in both basal (arrowheads) and ECM-detached (arrow) cells in $PERK^{\Delta/\Delta}$ tissues. (D) Upper and middle rows, images showing enhanced BimEL staining in $PERK^{\Delta/\Delta}$ versus control tissues. Insets show magnification details. The middle panels show strong BimEL staining of $PERK^{\Delta/\Delta}$ detached cells located within the lumen (arrows). Lower panels show cleaved caspase-3 staining in $PERK^{\Delta/\Delta}$ and control tissues, which displayed more cellularity than the KO mammary epithelium. Numbers in the lower left corners are the means ± standard errors of the means (SEM) of the percentages of cleaved caspase-3-positive luminal cells per field; ~1,000 total luminal cells were scored. Blue, hematoxylin and eosin (H&E) staining.

shown to be advantageous for tumors (4, 7). Because Fv2E-ΔNPERK activation caused luminal filling reminiscent of that observed during DCIS, we evaluated whether autophagy and PERK phosphorylation were differentially regulated in normal breast and DCIS tissues. We analyzed P-PERK and LC3 expression using immunohistochemistry in normal breast tissue and in DCIS and its benign adjacent tissue. Negative controls showed no staining (data available upon request). The P-PERK signal was low and homogeneous in normal breast epithelium or benign adjacent normal breast tissue (Fig. 8A and B), although it was upregulated in luminal cells (Fig. 8A, right panel). In contrast to the case for normal tissue, the P-PERK signal was highly increased and heterogeneous in DCIS tissue (Fig. 8C). The enhanced P-PERK signal was limited primarily to the epithelial tissue, and some regions of the DCIS lesions or individual cells showed dramatically increased P-PERK levels (Fig. 8C, right panel). The LC3 signal was also homogeneous in normal breast epithelium or benign adjacent normal breast tissue and, as predicted by our studies, it was found to be upregulated in luminal cells (Fig. 8D and E). In

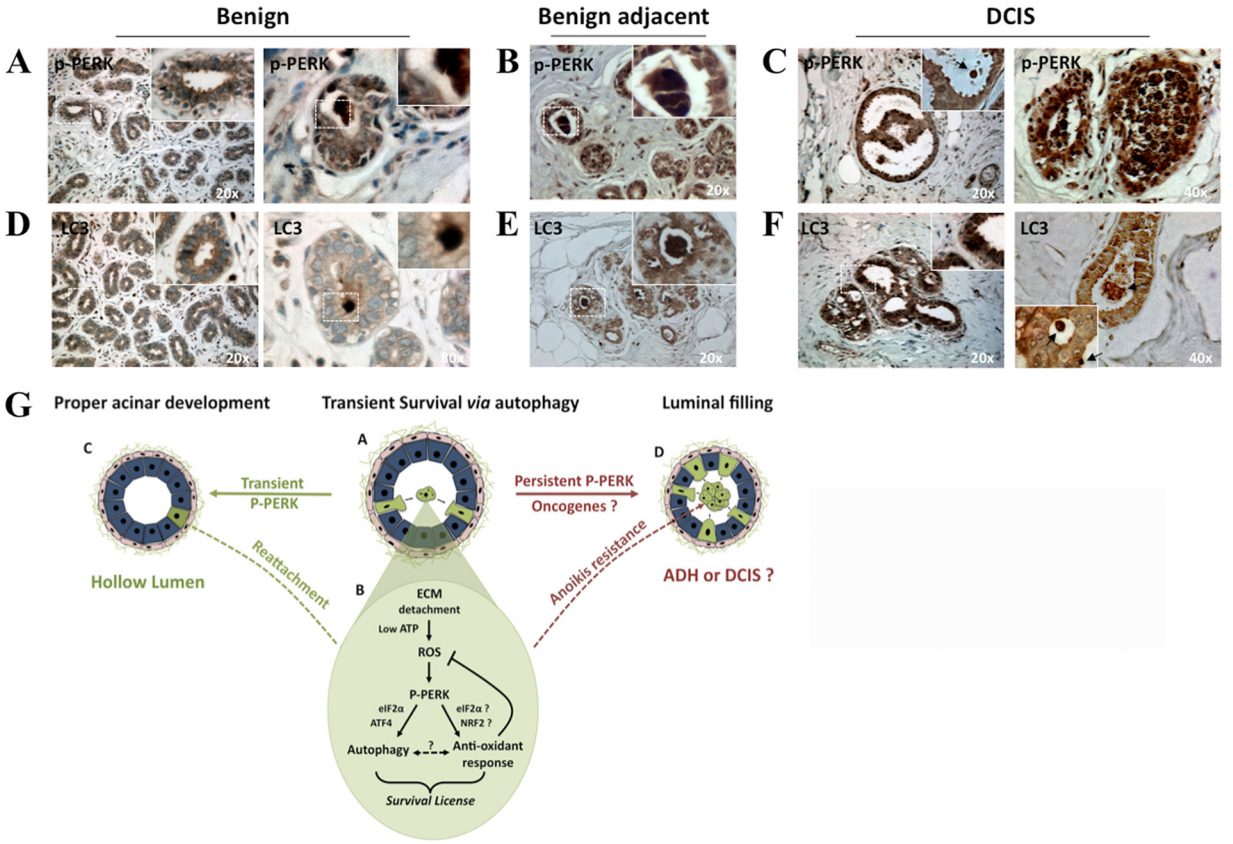

FIG. 8. PERK phosphorylation and LC3 expression in normal and DCIS tissues (A and F) and a model summarizing the findings (G). (A to C) Representative images of benign (A), benign adjacent (B), and DCIS (C) human mammary gland tissues embedded in paraffin blocks, sectioned, and stained with P-PERK Ab. The insets show detailed magnifications of lumens and detaching cells (arrow in panel C) with strong P-PERK. (D to F) Representative images of benign (D), benign adjacent (E), and DCIS (F) human mammary gland tissues embedded in paraffin blocks, sectioned, and stained with LC3 Ab. The insets show detailed magnifications of lumens and detaching cells (arrows in panel F) with enhanced LC3 staining. Blue, H&E staining. Total samples tested, $n = 5$; samples shown, $n = 2$. Patterns were similar in all 5 control or tumor tissues. (G) Model of PERK-induced survival during lumen formation. During mammary acinar development or tissue maintenance, MECs that become detached (A, green cells) activate a "survival license"-dependent PERK activation (B, pathway). Upon loss of adhesion, ROS accumulate due to low ATP production. PERK senses this signal, possibly due to misfolding on nascent proteins in the ER, and phosphorylates eIF2α. This in turn results in ATF4 and CHOP upregulation of autophagy genes such as ATG7 (B, autophagy), which promotes survival of suspended cells. Concomitantly, PERK, possibly through eIF2α→ATF4 or other transcription factors such as NRF2, induces genes that allow ROS detoxification via the upregulation of GSH (B, antioxidant response). Whether autophagy and antioxidant responses are interdependent is unclear at this time. During normal acinar development the "survival license" activated by PERK, which expires after 6 to 8 h, provides a window of opportunity for some luminal cells to resist anoikis, reattach, and contribute to the timely organization of a polarized acinus (C, hollow lumen). However, signals (e.g., oncogenes) that maintain activated PERK might hijack this "survival license" to make it permanent (D). This results in anoikis resistance and luminal occupancy, which might favor the progressive development of cancer lesions such as DCIS.

agreement with a previous report (15), DCIS tissue showed a clear enhancement in the overall LC3 signal, and this increased signal was more prominent in centrally located cells in the lesions (Fig. 8F). These data indicate that PERK activation and LC3 upregulation are concordant in normal, benign adjacent, and DCIS tissues; moreover, both of these signals are increased in DCIS tissues, with the highest levels of expression present in the centrally located cells of these preinvasive lesions.

DISCUSSION

Here we demonstrate that activation of the ER kinase PERK promotes the survival of luminal MECs detached from the ECM. Two recent studies have shown that upon loss of adhesion, MECs activate survival via autophagy (16) but also accumulate lethal ROS levels in association with reduced ATP production (40). We now demonstrate that suspension-induced PERK coordinately contributes to the induction of autophagy, the maintenance of ATP production, and the stimulation of a ROS detoxification response. The last most likely allows for autophagy to proceed and protect cells until adhesion is restored. In a 3D morphogenesis model, the enforced activation of PERK results in the aberrant survival and accumulation of cells in the luminal space, indicating that this pathway must be turned off during morphogenesis for proper luminal clearance. The tissue-specific deletion of PERK in the mouse mammary gland tissue results in reduced autophagy and increased apoptosis, whereas both PERK phosphorylation and au-

tophagy are concomitantly increased in human DCIS. Based on these results, we propose that the proautophagic and antioxidant functions of PERK that operate during normal mammary acinar development are subverted in breast tumor cells to survive oxidative stress and resist anoikis.

Autophagy was found to protect luminal MECs lacking ECM contact in an ATG5- and ATG7-dependent manner (16), but the precise signals triggering this prosurvival mechanism in ECM-detached cells remain largely unclear (9). Here we show that PERK is an upstream inducer of detachment-induced autophagy. Interestingly, our data implicate the canonical PERK-eIF2α signaling axis as an important transcriptional regulator of multiple autophagy regulators (ATGs) involved in the early steps of autophagosome formation, including ATG5, ATG6/Beclin-1, and ATG8 expression. Among these, ATG6/Beclin1 was the most responsive ATG gene induced by PERK and its downstream effectors. Because transcription of these ATG genes is likely not sufficient to drive autophagy, it is possible that these core components of the autophagy machinery are also subject to posttranscriptional control downstream of PERK activation. Nonetheless, in addition to the induction of these ATG transcripts, our results also demonstrate that PERK activation (using a control dimerization strategy to activate this ER kinase) is sufficient to promote bona fide autophagic degradation. Notably, PERK may directly or indirectly affect other pathways important in autophagy induction, such as the energy-sensing LKB1-AMPK pathway, which is activated when AMP levels increase and consequently leads to both mTOR inhibition (18) and autophagy activation (29). Further examination of this salient issue remains a important topic for future study.

In MCF10A 3D cultures, enforced PERK activation during the late stages of morphogenesis allowed viable MECs devoid of any ECM (i.e., surface bound laminin-5) to persistently occupy the luminal space. This phenotype was dependent on ATF4 and ATG7 and ultimately resulted in increased acinar basal cell numbers, suggesting that surviving MECs reattached to the ECM in the basal layer of cells. Luminal MEC survival was reversed by chloroquine, which blocks fusion of autophagosomes to lysosomes (25). Thus, drugs that interrupt PERK-induced autophagy might have antitumor effects. In agreement with this, chloroquine was shown to limit the survival of breast cancer cells (15). We conclude that PERK can protect against anoikis and that oncogenic signals that perpetuate PERK activation might promote unwanted MEC survival.

Based on these results, one can speculate that PERK ensures that a MEC inefficiently attached survives via autophagy until proper adhesion is restored. Importantly, we found that these functions of PERK appear to be operational *in vivo*. During lactation, mouse mammary epithelial tissue where PERK was conditionally deleted showed an absence of P-PERK signal that was associated with reduced autophagosomes (e.g., LC3 staining). In further support of this, we found that in normal reduction mammoplasty and benign adjacent human tissues, PERK activation was enhanced and LC3-associated autophagy was increased primarily in luminal cells, once again suggesting an anoikis resistance mechanism. Furthermore, in DCIS lesions, where anoikis resistance is thought to lead to luminal filling (11), strong PERK phosphorylation was associated with prominent LC3 staining. In agreement with our findings, a recent study demonstrated that autophagy is upregulated in DCIS lesions, but the link to PERK was not delineated (15).

In addition to the induction of autophagy, PERK senses the accumulation of ROS in suspended cells and induces an antioxidant response dependent on eIF2α phosphorylation (41). During ECM detachment, this response includes the induction of the glycine transporter Glyt1 and the x(c)-cystine/glutamate exchanger Slc3a2, which is required to transport cystine that upon reduction is converted into the glutathione (GSH) precursor cysteine (22, 23). These genes are part of the PERK antioxidant response mediated by ATF4, and GSH is a major reducing agent that prevents ROS-mediated damage (6, 28). PERK can also maintain cellular redox homeostasis through the activation of Nrf2 (8), which is a PERK substrate and a central regulator of GSH metabolism (42, 43). In fact, in ErbB2/Neu-driven tumors, PERK-activated Nrf2 is the primary antioxidant response regulator (4). Thus, we cannot exclude the possibility that PERK-Nrf2 signaling might contribute to decrease ROS levels in suspended cells. NAC was sufficient to reduce PERK activation and LC3 processing, suggesting that the accumulated ROS and possibly misfolding of proteins leads to PERK activation. The latter is needed to reduce ROS because expression of a PERKΔC or eIF2α Ser51 Ala mutant resulted in increased ROS accumulation and reduced plating efficiency. Further, PERK activation in Fv2E-ΔNPERK-expressing acini completely reversed ROS accumulation. We previously showed that neither PKR nor GCN2 is activated in suspension (41), reinforcing our findings that this is a PERK-dependent mechanism. Our finding that PERK executes a survival program during mammary acinus morphogenesis in both mouse and human normal tissues and human tumor tissues is significant, as it reveals a potential new role under normal and/or pathophysiological conditions.

PERK has a dual function in mouse mammary epithelium (3, 5, 41). It can prevent tumorigenesis in aging animals, but it also can aid ErbB2/Neu transformation (5). The former is in agreement with our previous findings (41) that if PERK is inhibited using dominant-negative alleles, MECs, but primarily the basal ECM-attached acinar cells, engage in enhanced proliferation and tumor formation. While we had shown that PERK signaling occurred in luminal cells, we had not identified its function at that time (41). We also found that PERK activation induced p21 and p27 (data not shown), suggesting that its survival function might be tied to a transient growth arrest to promote damage relief. Thus, the growth-suppressive and antioxidant functions of PERK may be necessary to prevent MECs from accumulating damage that can lead to transformation. Importantly, if the transforming signal is an oncogene product like ErbB2, PERK serves as a survival factor allowing tumors to cope with ROS, hypoxia, and ER stress (5). It is possible that the oncogenic signal is sufficient to overcome PERK-induced cell cycle arrest, leaving the prosurvival function to assist tumorigenesis. We propose that the mechanism of survival normally induced by PERK in luminal cells is hijacked to protect transformed MECs from anoikis.

In suspended cells, a canonical PERK pathway is activated (reference 41 and this study). However, the precise control of PERK activation during ECM detachment remains unclear. One study showed that loss of adhesion of MCF10A cells results in reduced glucose transport, a drop in ATP production, and increased ROS. It is possible that the ER protein-folding machinery, which is ATP dependent, is highly sensitive to the ATP drop

and that luminal suspended MECs accumulate misfolded proteins in the ER, resulting in PERK activation as part of a UPR. However, ECM detachment does not appear to induce a canonical UPR, because Grp78, Hsp47, and Erp72/PDI, as well as XBP-1 splicing, is not induced during the same time frame in which PERK activation promotes survival (41). Although unknown, it may also be possible that suspended MECs, due to altered cell polarity, disrupt vesicular transport, leading to ER client protein accumulation and PERK activation.

In summary, we have found that PERK controls two mechanisms that become simultaneously activated in ECM-detached cells and dictate cell fate: prodeath ROS induction that is antagonized by PERK and a prosurvival autophagy response that is promoted by PERK. We propose that because cell detachment is a critical stress condition, the simultaneous activation of these pathways represents a safeguard mechanism. In the initial hours after detachment, PERK "licenses" suspended cells for survival by inducing autophagy and ROS detoxification, allowing cells to reattach, resolve both autophagy induction and ROS stress, and resume normal functions (Fig. 8G). If MECs do not attach to the ECM, then ROS stress is insurmountable and apoptotic pathways takes over to fully commit these delocalized cells to death via anoikis. We are currently dissecting how transformed mammary epithelial cells hijack these prosurvival functions of PERK during anoikis to provide a robust and persistent anoikis resistance phenotype.

ACKNOWLEDGMENTS

We are grateful to Sharon Sequeira (SUNY—Albany) for development of the eIF2α mutant cell lines and to Huei-Chi Wen for help with caspase-3 and p-Rb stainings.

Confocal laser scanning microscopy was performed at the Microscopy Shared Resources Facility (MSSM), supported with funding from NIH-NCI shared resources grant 5R24CA095823-04, NSF Major Research Instrumentation grant DBI-9724504, and NIH shared instrumentation grant 1 S10RR0 9145-01). This work is supported by grants from the Samuel Waxman Cancer Research Foundation Tumor Dormancy Program, NIH/National Cancer Institute (CA109182), NIEHS (ES017146), and NYSTEM to J.A.A-G, NIH RO1 CA126792 and CA126792-S1 (ARRA) to J.D., and P01 CA104838 and a Leukemia & Lymphoma Scholar award to J.A.D.

REFERENCES

1. **Barone, M. V., A. Crozat, A. Tabaee, L. Philipson, and D. Ron.** 1994. CHOP (GADD153) and its oncogenic variant, TLS-CHOP, have opposing effects on the induction of G1/S arrest. Genes Dev. **8:**453–464.
2. **Bi, M., et al.** 2005. ER stress-regulated translation increases tolerance to extreme hypoxia and promotes tumor growth. EMBO J. **24:**3470–3481.
3. **Blais, J. D., et al.** 2006. Perk-dependent translational regulation promotes tumor cell adaptation and angiogenesis in response to hypoxic stress. Mol. Cell. Biol. **26:**9517–9532.
4. **Bobrovnikova-Marjon, E., et al.** 2010. PERK promotes cancer cell proliferation and tumor growth by limiting oxidative DNA damage. Oncogene **29:**3881–3895.
5. **Bobrovnikova-Marjon, E., et al.** 2008. PERK-dependent regulation of lipogenesis during mouse mammary gland development and adipocyte differentiation. Proc. Natl. Acad. Sci. U. S. A. **105:**16314–16319.
6. **Chakravarthi, S., C. E. Jessop, and N. J. Bulleid.** 2006. The role of glutathione in disulphide bond formation and endoplasmic-reticulum-generated oxidative stress. EMBO Rep. **7:**271–275.
7. **Chen, N., and J. Debnath.** 2010. Autophagy and tumorigenesis. FEBS Lett. **584:**1427–1435.
8. **Cullinan, S. B., et al.** 2003. Nrf2 is a direct PERK substrate and effector of PERK-dependent cell survival. Mol. Cell. Biol. **23:**7198–7209.
9. **Debnath, J.** 2008. Detachment-induced autophagy during anoikis and lumen formation in epithelial acini. Autophagy **4:**351–353.
10. **Debnath, J., and J. S. Brugge.** 2005. Modelling glandular epithelial cancers in three-dimensional cultures. Nat. Rev. Cancer **5:**675–688.
11. **Debnath, J., et al.** 2002. The role of apoptosis in creating and maintaining luminal space within normal and oncogene-expressing mammary acini. Cell **111:**29–40.
12. **Debnath, J., S. K. Muthuswamy, and J. S. Brugge.** 2003. Morphogenesis and oncogenesis of MCF-10A mammary epithelial acini grown in three-dimensional basement membrane cultures. Methods **30:**256–268.
13. **Dennis, P. B., and C. A. Mercer.** 2009. The GST-BHMT assay and related assays for autophagy. Methods Enzymol. **452:**97–118.
14. **Denoyelle, C., et al.** 2006. Anti-oncogenic role of the endoplasmic reticulum differentially activated by mutations in the MAPK pathway. Nat. Cell Biol. **8:**1053–1063.
15. **Espina, V., et al.** 2010. Malignant precursor cells pre-exist in human breast DCIS and require autophagy for survival. PLoS One **5:**e10240.
16. **Fung, C., R. Lock, S. Gao, E. Salas, and J. Debnath.** 2008. Induction of autophagy during extracellular matrix detachment promotes cell survival. Mol. Biol. Cell **19:**797–806.
17. **Gilmore, A. P.** 2005. Anoikis. Cell Death Differ. **12**(Suppl. 2):1473–1477.
18. **Hardie, D. G.** 2004. The AMP-activated protein kinase pathway—new players upstream and downstream. J. Cell Sci. **117:**5479–5487.
19. **Harding, H. P., Y. Zhang, A. Bertolotti, H. Zeng, and D. Ron.** 2000. Perk is essential for translational regulation and cell survival during the unfolded protein response. Mol. Cell **5:**897–904.
20. **Harding, H. P., Y. Zhang, and D. Ron.** 1999. Protein translation and folding are coupled by an endoplasmic-reticulum-resident kinase. Nature **397:**271–274.
21. **Hebner, C., V. M. Weaver, and J. Debnath.** 2008. Modeling morphogenesis and oncogenesis in three-dimensional breast epithelial cultures. Annu. Rev. Pathol. **3:**313–339.
22. **Howard, A., et al.** 2010. Glycine transporter GLYT1 is essential for glycine-mediated protection of human intestinal epithelial cells against oxidative damage. J. Physiol. **588:**995–1009.
23. **Huang, Y., Z. Dai, C. Barbacioru, and W. Sadee.** 2005. Cystine-glutamate transporter SLC7A11 in cancer chemosensitivity and chemoresistance. Cancer Res. **65:**7446–7454.
24. **Kim, K. W., L. Moretti, L. R. Mitchell, D. K. Jung, and B. Lu.** 2010. Endoplasmic reticulum stress mediates radiation-induced autophagy by perk-eIF2alpha in caspase-3/7-deficient cells. Oncogene **29:**3241–3251.
25. **Klionsky, D. J., A. M. Cuervo, and P. O. Seglen.** 2007. Methods for monitoring autophagy from yeast to human. Autophagy **3:**181–206.
26. **Komatsu, M., et al.** 2007. Homeostatic levels of p62 control cytoplasmic inclusion body formation in autophagy-deficient mice. Cell **131:**1149–1163.
27. **Kouroku, Y., et al.** 2007. ER stress (PERK/eIF2alpha phosphorylation) mediates the polyglutamine-induced LC3 conversion, an essential step for autophagy formation. Cell Death Differ. **14:**230–239.
28. **Lewerenz, J., and P. Maher.** 2009. Basal levels of eIF2alpha phosphorylation determine cellular antioxidant status by regulating ATF4 and xCT expression. J. Biol. Chem. **284:**1106–1115.
29. **Liang, J., et al.** 2007. The energy sensing LKB1-AMPK pathway regulates p27(kip1) phosphorylation mediating the decision to enter autophagy or apoptosis. Nat. Cell Biol. **9:**218–224.
30. **Lock, R., and J. Debnath.** 2008. Extracellular matrix regulation of autophagy. Curr. Opin. Cell Biol. **20:**583–588.
31. **Lu, P. D., et al.** 2004. Cytoprotection by pre-emptive conditional phosphorylation of translation initiation factor 2. EMBO J. **23:**169–179.
32. **Milani, M., et al.** 2009. The role of ATF4 stabilization and autophagy in resistance of breast cancer cells treated with Bortezomib. Cancer Res. **69:**4415–4423.
33. **Ogata, M., et al.** 2006. Autophagy is activated for cell survival after endoplasmic reticulum stress. Mol. Cell. Biol. **26:**9220–9231.
34. **Park, M. A., et al.** 2008. Regulation of autophagy by ceramide-CD95-PERK signaling. Autophagy **4:**929–931.
35. **Pearson, G. W., and T. Hunter.** 2007. Real-time imaging reveals that non-invasive mammary epithelial acini can contain motile cells. J. Cell Biol. **179:**1555–1567.
36. **Ranganathan, A. C., L. Zhang, A. P. Adam, and J. A. Aguirre-Ghiso.** 2006. Functional coupling of p38-induced up-regulation of BiP and activation of RNA-dependent protein kinase-like endoplasmic reticulum kinase to drug resistance of dormant carcinoma cells. Cancer Res. **66:**1702–1711.
37. **Rouschop, K. M., et al.** 2010. The unfolded protein response protects human tumor cells during hypoxia through regulation of the autophagy genes MAP1LC3B and ATG5. J. Clin. Invest. **120:**127–141.
38. **Rutkowski, D. T., and R. J. Kaufman.** 2004. A trip to the ER: coping with stress. Trends Cell Biol. **14:**20–28.
39. **Rzymski, T., et al.** 2010. Regulation of autophagy by ATF4 in response to severe hypoxia. Oncogene **29:**4424–4435.
40. **Schafer, Z. T., et al.** 2009. Antioxidant and oncogene rescue of metabolic defects caused by loss of matrix attachment. Nature **461:**109–113.
41. **Sequeira, S. J., et al.** 2007. Inhibition of proliferation by PERK regulates mammary acinar morphogenesis and tumor formation. PLoS One **2:**e615.
42. **Wild, A. C., H. R. Moinova, and R. T. Mulcahy.** 1999. Regulation of gamma-glutamylcysteine synthetase subunit gene expression by the transcription factor Nrf2. J. Biol. Chem. **274:**33627–33636.
43. **Wild, A. C., and R. T. Mulcahy.** 2000. Regulation of gamma-glutamylcysteine synthetase subunit gene expression: insights into transcriptional control of antioxidant defenses. Free Radic. Res. **32:**281–301.